All-Cellulose Composite

Takashi Nishino,* Ikuyo Matsuda, and Koichi Hirao

Department of Chemical Science and Engineering, Faculty of Engineering, Kobe University, Rokko, Nada, Kobe 657-8501, Japan

Received April 9, 2004; Revised Manuscript Received June 21, 2004

ABSTRACT: An *all*-cellulose composite, in which both the fibers and the matrix are cellulose, was prepared by distinguishing the solubility of the matrix cellulose into the solvent from that of the fibers through pretreatment. The structure, mechanical, and thermal properties of this composite were investigated using an X-ray diffraction, a scanning electron microscope, a tensile test, and dynamic viscoelastic and thermomechanical analyses. The tensile strength of uniaxially reinforced all-cellulose composite was 480 MPa at 25 °C, and the dynamic storage modulus was as high as 20 GPa at 300 °C. These were comparable or even higher than those of conventional glass-fiber-reinforced composites. In addition, a linear thermal expansion coefficient was about 10^{-7} K^{-1}. This all-cellulose composite shows substantial advantages, that is, it is composed of sustainable resources, there is less interface between the fiber and the matrix, it possesses excellent mechanical and thermal performance during use, and it is biodegradable after the service.

Introduction

Composite materials, typically glass fibers or carbon fibers embedded into epoxy resin or unsaturated polyester, show excellent mechanical and thermal properties; thus, they are widely used in various applications ranging from aerospace to vehicles to sports utensils.[1] However, these advantages cause environmental problems when disposing by incineration. Consequently, there are growing demands for environmentally friendly composites.[2]

Cellulose is a natural linear polysaccharide in which *D*-glucopyranose rings are connected to one another with β-(1→4)-glycosidic links. Cellulose is the most abundant biomass resource and possesses excellent mechanical and thermal properties. Natural cellulose (cellulose I) also boasts an elastic modulus, E_l, of 138 GPa for the crystalline regions in the direction parallel to the chain axis.[3] This is comparable with the E_l values of high performance synthetic fibers such as poly(*p*-phenylene terephthalamide) (156 GPa, Kevlar, Twaron), Vectran (126 GPa), Technora (88 GPa), and Ekonol (130 GPa).[4] In addition, the maximum macroscopic Young's modulus of natural plant cellulose (up to 128 GPa)[5] is higher than those of aluminum (70 GPa) and glass fibers (76 GPa). The ultimate tensile strength of cellulose is estimated to be 17.8 GPa.[7] This is 7 times higher than that of steel. Intrinsically, the very high elastic modulus and tensile strength (not specific modulus and specific strength) imply that cellulose possesses the potential to replace glass fiber, and it shows promise as a reinforcement fiber for composites where the density is not a concern. Current trends toward environmentally friendly composites focus on the use of cellulose fibers.[6]

Usually, composites are composed of two chemically foreign components, so there should be an interface between the fiber and the matrix. The interface often brings serious problems such as poor adhesion and water uptake by the composites. On the other hand, when the fiber and the matrix are composed of the same material, some benefits relevant to recyclability, and a better adhesion at interface, can be expected. In this point of view, *all*-polyethylene (PE) composite[8] and *all*-polypropylene (PP) composite[9,10] have been recently investigated. The biggest problem with manufacturing these types of composites is that the incorporated fibers also overheat and lose their high-performance characteristics during processing of the melted matrix. Dealing with this problem, for example, high-density PE fibers (melting point T_m = 145 °C) are combined with low-density PE (T_m = 120 °C), and an all-PE composite is processed in the temperature window between both T_m's.

Cellulose is well known not to melt, but shows thermal degradation at high temperature. Therefore, to process cellulose, we have to employ a wet process. Natural cellulose can be dissolved into *N*, *N*′-dimethyl acetamide (DMAc) containing LiCl through the coordination of Li ions to the hydroxyl groups of cellulose.[11] However, pretreatment is needed for dissolution. In other words, native cellulose does not dissolve in this solvent without being pretreated. In this study, this solubility difference was used here to impregnate the native cellulose fibers into the cellulose matrix. The structure, mechanical, and thermal properties of this *all*-cellulose composite were investigated.

Experimental Section

Sample Preparation. The cellulose fiber used in this study is refined ramie supplied from Toyobo Co., Ltd. For the matrix, craft pulp from coniferous trees, supplied from Oji Paper Co., Ltd., was pretreated. The pretreatment was performed by immersing the pulp in distilled water, acetone, and DMAc, each for 24 h at 25 °C, successively. No structural change of the pulp was observed after experiencing this pretreatment judging from an X-ray diffraction profile and a scanning electron micrograph. Then, the pretreated pulp was dissolved in DMAc containing LiCl (8 wt %) solvent with a cellulose concentration of 3 wt %. Non-pretreated ramie fibers were aligned parallel one another and fixed at both ends, followed by being impregnated with the cellulose solution under a reduced pressure. The solution started gelation by exposing it to an ambient condition for 12 h. After another 12 h, the fiber-incorporated gel was immersed into methanol to extract

* Address correspondence to this author. Tel: +81-78-803-6164; fax: +81-78-803-6198; e-mail: tnishino@kobe-u.ac.jp.

10.1021/ma049300h CCC: $27.50
Published on Web 09/11/2004

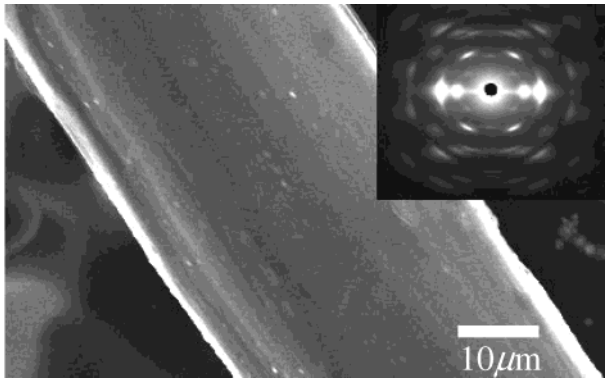

Figure 1. Scanning electron micrographs of the single ramie fiber. The corner X-ray fiber photograph was taken by irradiating Cu Kα radiation to the fiber in the direction perpendicular to the fiber orientation.

DMAc and LiCl, then dried at room temperature for 12 h, and further dried in a vacuum at 60 °C for 24 h. The specimen was a rectangular strip (dimensions: 40 mm × 30 mm × thickness 1 mm) with a fiber volume fraction of 80%.

Measurements. X-ray diffraction photographs were taken by a flat camera with a camera length of 37.5 mm. The Cu Kα radiation, generated with RINT-2000 (Rigaku Co.) at 40 kV, 20 mA, was irradiated on the specimen perpendicular to the fiber orientation. The equatorial diffraction profile was detected using an X-ray goniometer with a symmetric reflection geometry. After subtracting an air scattering, the diffraction profile was curve resolved into noncrystalline part and crystalline reflections by curve fitting. In this study, the profile of the matrix cellulose was regarded as the noncrystalline part. Then, the integral width of the 200 reflection was corrected for the CuKα doublet and an instrumental broadening. The crystallite size D was estimated using Scherrer's equation:[12]

$$D = \lambda/\beta \cdot \cos\theta$$

where λ = 1.5418 Å, β: corrected integral width, θ: Bragg angle for the 200 reflection.

The fiber surface, the cross section, and the fracture surface of the composite were observed using a scanning electron microscope, SEM, JSM-5610LVS (JEOL) at an accelerating voltage of 15 kV. Pt/Pd was deposited on the surface prior to the observation.

The stress−strain curves of the single ramie fiber, the cellulose matrix, and all-cellulose composite were measured using a tensile tester, Autograph AGS-1kND (Shimadzu), at 25 °C; the initial length of the specimen was 20 mm and the extension rate was 20 mm/min. The cross-sectional area of the single fiber was determined by measuring the weight, the length, and the density. The numbers of tested specimens were 30 for the single ramie fiber and 5 for the composite. The average values and standard deviations of Young's modulus and tensile strength σ_{max} were evaluated. Dynamic storage modulus was measured by a dynamic mechanical analyzer, DVA-220S (ITK Ltd.), from 25 to 300 °C. The measurements were performed under nitrogen atmosphere to avoid thermal oxidation. A heating rate of 6 °C/min, an original length of 10 mm, and a frequency of 10 Hz were employed. The tensile deformation (0.25%) was applied to the specimen in the direction parallel to the fiber orientation.

Thermomechanical analysis was performed using a thermomechanical analyzer, TMA-SS120S (Seiko Instruments), at a heating rate of 10 °C/min. The specimen with an original length of 15 mm was subjected to a uniaxial stress of 0.12 MPa.

Prior to all measurements, the specimen was conditioned at 120 °C for 1 h.

Results and Discussion

Figure 1 shows the scanning electron micrograph and the X-ray fiber photograph of ramie fiber. The fiber surface was smooth, and an average diameter was around 30 microns. From the X-ray fiber photograph, the ramie fiber showed high crystallinity and a high degree of the crystallite orientation.

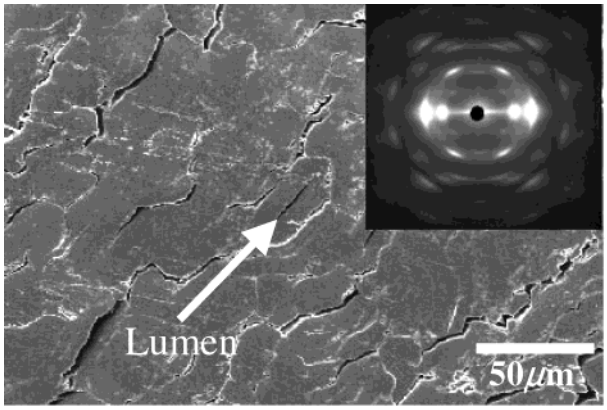

Figure 2. Scanning electron micrograph of the cross section of all-cellulose composite. The corner X-ray diffraction photograph was taken by irradiating Cu Kα radiation to the composite in the direction perpendicular to the fiber orientation.

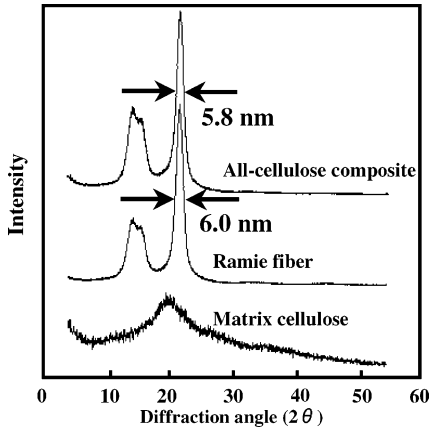

Figure 3. Equatorial X-ray diffraction profiles of all-cellulose composite, ramie fiber, and the matrix cellulose.

Figure 2 shows the SEM micrograph of the cross section of the all-cellulose composite. The X-ray diffraction photograph at the corner was taken from the direction perpendicular to the fiber orientation. The SEM micrograph indicates that the ramie fibers were surrounded by the matrix cellulose, and lumen (hollow microtube inside the native plant fiber) was observed. This shows that cellulose fibers were totally impregnated, and an all-cellulose composite could be produced. The X-ray diffraction photograph of the composite clearly showed a specifically uniaxially oriented fiber pattern with high crystallinity. Comparing with the diffraction pattern of ramie fiber (Figure 1), high crystallite orientation was maintained in the all-cellulose composite.

Figure 3 shows the equatorial diffraction profiles of ramie fiber, the all-cellulose composite, and the matrix cellulose. Ramie fiber belongs to cellulose I, which is typical for natural plant cellulose.[13] This crystal modification was also sustained in the composite. There was no change in the crystallite size of ca. 6 nm for the 200 reflection before and after impregnation. These results reveal that the incorporated ramie fibers were not damaged in the composite. On the other hand, the matrix cellulose was converted into noncrystalline condition through dissolution and re-solidification.

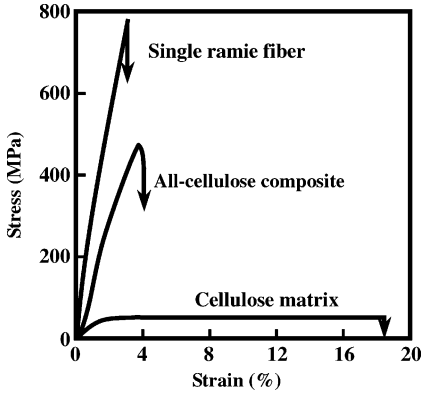

Figure 4. Stress−strain curve of all-cellulose composite together with those of single ramie fiber and the matrix cellulose.

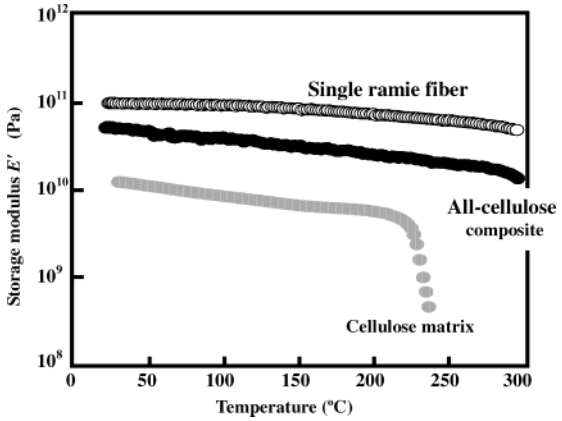

Figure 5. Temperature dependence of the dynamic storage modulus E' of all-cellulose composite, together with those of the single ramie fiber and the matrix cellulose.

Figure 4 shows the stress−strain curve of the all-cellulose composite together with those of typical single ramie fiber and the matrix cellulose. A single ramie fiber possesses a high Young's modulus (average value = 42 GPa; standard deviation = 9 GPa) and high tensile strength (average σ_{max} = 730 MPa; standard deviation = 190 MPa). Compared with them, Young's modulus and tensile strength were lower for the all-cellulose composite. However, the average σ_{max} of 480 MPa (standard deviation = 50 MPa) for the all-cellulose composite was comparable or even higher than that of conventional glass-fiber-reinforced composites. The matrix showed low modulus, low strength, and high elongation at break. These will be due to noncrystalline feature of the matrix cellulose as shown in Figure 3.

Figure 5 shows the temperature dependencies of a dynamic storage modulus E' of the all-cellulose composite, together with those of the typical single fiber and the matrix cellulose. The E' value of ramie fiber decreased from 87 GPa at 20 °C to 45 GPa at 300 °C. The Young's modulus, Y, of the conventional glass-fiber-reinforced composite (GFRP; fiber content = 50%) lies between 6.7 GPa (Reuss model: $Y = [(0.5/Y_m) + (0.5/Y_f)]^{-1}$) and 40 GPa (Voigt model: $Y = 0.5\ Y_m + 0.5 Y_f$), assuming Y_m (Young's modulus of matrix epoxy resin) = 3.5 GPa and Y_f (Young's modulus of E-glass fiber) = 76 GPa, respectively.[14] The E' value of the all-cellulose composite was 45 GPa at 25 °C, which is higher than the above-mentioned Young's modulus of GFRP. Furthermore, even though the E' value of the all-cellulose composite decreased with temperature, the drop was limited to 20 GPa at 300 °C. This thermal/mechanical performance characteristic is extremely high among polymer-based composites, and it originates from the intrinsically excellent properties of the ramie fibers themselves.

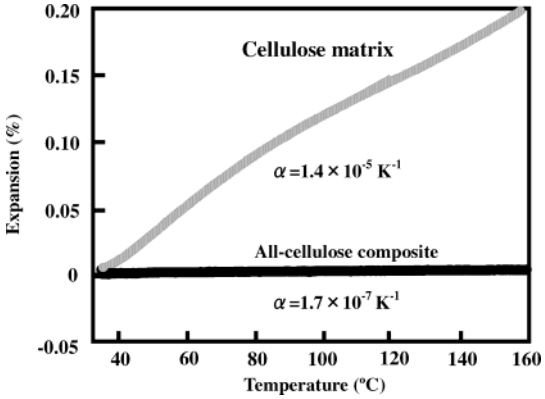

Figure 6. Temperature dependence of the linear thermal expansion of all-cellulose composite, together with that of the matrix cellulose.

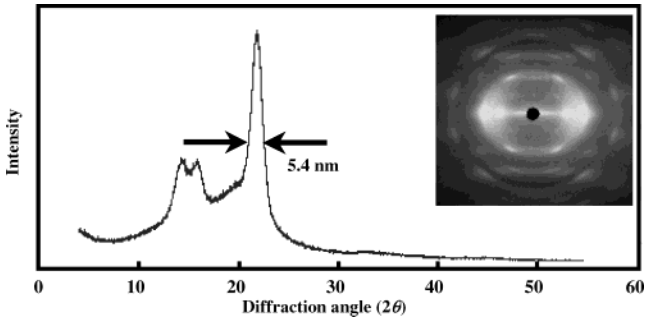

Figure 7. Equatorial X-ray diffraction profile of all-cellulose composite with pretreated fibers. The corner X-ray diffraction photograph was taken by irradiating Cu K_α radiation to the composite in the direction perpendicular to the fiber orientation.

Figure 6 shows the linear thermal expansion behavior of the all-cellulose composite, together with that of the matrix cellulose. The cellulose matrix showed thermal expansion with increasing temperature, and its linear thermal expansion coefficient, α, is 1.4×10^{-5} K^{-1}. In contrast, the all-cellulose composite showed apparently almost no thermal expansion or contraction; the α value of the composite was about 10^{-7} K^{-1}, which is much lower than those of metals (for example, Fe: 11.8×10^{-6} K^{-1}, Si: 2.49×10^{-6} K^{-1}, respectively).[15]

As revealed from the SEM micrograph in Figure 2, the interfacial cracks were observed between the fiber and the matrix. This suggests that the interface did not completely diminish but still existed in the all-cellulose composite shown above. To prepare the interfaceless composite, the incorporated fibers were also pretreated followed by being impregnated into cellulose solution. By this method, the fiber surface would be partially swollen or dissolved, and the interdiffusion of cellulose molecules across the interface was expected to be stimulated.

Figure 7 shows the equatorial diffraction profile of the all-cellulose composite with pretreated fibers, together with the X-ray diffraction photograph. In this case, the pretreated fibers were in contact with cellulose solution for 24 h till immersing the fiber incorporated gel into methanol. The crystallite size for the 200 reflection of the incorporated fiber decreased to 5.4 nm (cf. 6 nm for

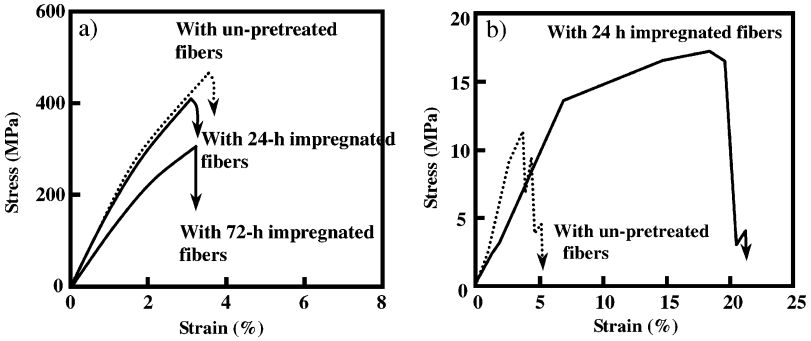

Figure 8. Stress−strain curves of all-cellulose composites (broken line) with un-pretreated fibers and (solid line) with pretreated and impregnated fibers in the direction (a) parallel and (b) perpendicular to the fiber orientation. The impregnation periods were 24 and 72 h, respectively.

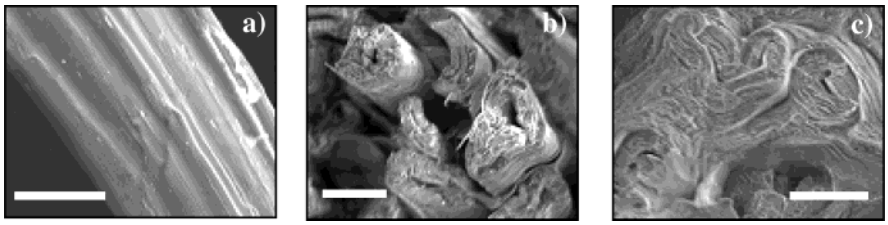

Figure 9. Scanning electron micrographs of (a) the pretreated and 72-h impregnated single ramie fiber, and the fracture surface of all-cellulose composites (b) with un-pretreated fibers and (c) with pretreated and 24-h impregnated fibers. The scale bars were equal to 20 μm.

the as-received ramie fiber, Figure 3) through the processing of the composite. The X-ray diffraction photograph showed that the intensity of the noncrystalline scattering increased, but the high crystallite orientation of cellulose I was sustained in this composite. The apparent crystallinity of as-supplied ramie fiber was 82%; it decreased to 65% in this composite. This indicates that the noncrystalline region increased 17% for the all-cellulose composite with pretreated fibers. Therefore, the surface of the pretreated fibers were partially dissolved into the solvent, which contributes the interdiffusion of cellulose molecules across the fiber/matrix interface; however, the crystal system of the remained core part of the fiber was maintained as cellulose I.

Figure 8 shows the stress−strain curves of the all-cellulose composite with pretreated fibers in the direction (a) parallel and (b) perpendicular to the fiber direction. The impregnation periods till the fiber incorporated gel into methanol were chosen as 24 and 72 h, respectively. Compared with the result for the all-cellulose composite with unpretreated fibers (broken line), the longer impregnation period (72 h) seems to bring the decrease of tensile strength and Young's modulus for the composite. These will be due to the overdissolving of the fiber during the impregnation, which destroyed the mechanical high performance of the incorporated fibers. Partial dissolving of the fiber was clear from Figure 9 a, where the fiber surface was roughened during impregnation. On the contrary, by choosing the optimum impregnation period (24 h), the mechanical properties of the composite with pretreated and 24-h impregnated fibers were maintained almost as same as those of the composite with un-pretreated fibers (Figure 8a). The SEM micrographs of the fracture surface after the tensile test along the fiber direction were shown in Figure 9 for the composites (b) with un-pretreated fibers and (c) with pretreated and 24-h impregnated fibers, respectively. For the composite with pretreated and 24-h impregnated fibers, the simultaneous breakage of both the fibers and the matrix occurred, and lumens could be observed (Figure 9c). This implies a strong adhesion between the fibers and the matrix, and the interface became obscure through the interdiffusion. In contrast, for the fracture surface of the composite with un-pretreated fibers (Figure 9b), fiber pullout from the matrix was obvious. From Figure 8b, the transverse tensile strength, Young's modulus, and the elongation at break were lower than those in the parallel direction because of high anisotropy of the fiber alignment in the composite. Even though, these mechanical properties were higher for the composite with pretreated and 24-h impregnated fibers. These were attributed to the increased interfacial strength resulting from the partial surface dissolving of the pretreated fiber/interdiffusion across the interface.

Conclusions

All-cellulose composite was manufactured with the wet process by controlling the solubility of cellulose through pretreatment conditions. This composite is totally composed of sustainable cellulosic resources, so it can be biodegradable after service. The uniaxially reinforced composite, in other words, the cellulose self-reinforced composite, possessed excellent mechanical and thermal properties during use. This composite can be used as an alternative of the glass-fiber-reinforced composite. By choosing the pretreatment condition to the fiber, the transverse mechanical properties of the composite was also enhanced through the molecular diffusion across the interface between the fiber and the matrix.

Acknowledgment. Ramie fibers and pulp were kindly supplied by Toyobo Co., Ltd., and Oji Paper Co., Ltd., respectively. The authors acknowledge the financial support of Sekisui Integrated Research Inc. and the Mazda Foundation's Research Grand.

References and Notes

(1) Hull, D.; Clyne, T. W. *An Introduction to Composite Materials*, 2nd ed.; Cambridge University Press: Cambridge, U.K., 1996.
(2) Mohanty, A. K.; Misra M.; Drzal, L. T. *J. Polym., Environment* **2002**, *10*, 19.
(3) Nishino, T.; Takano, K.; Nakamae, K. *J. Polym. Sci., Part B: Polym. Phys.* **1995**, *33*, 1647.
(4) Nakamae, K.; Nishino, T.; Shimizu, Y.; Matsumoto, T. *Polym. J.* **1987**, *19*, 451.
(5) Page, D. T.; El-Hosseiny, F.; Winker, K. *Nature* **1971**, *229*, 252.
(6) Ito, T. In *High Performance Polymer Composites*, Soc. Polym. Sci. *Jpn., Ed.*; Maruzen: Tokyo, 1990; Chapter 2 (in Japanese).
(7) Bledzki, A. K.; Gassan, J. *Prog. Polym. Sci.* **1999**, *24*, 221.
(8) Schulte, K.; Lacroix, F. V. In *Polymer Matrix Composites*; Talreja, R., Manson, J.-A. E., Eds.; Elsevier: Oxford, U.K., 2001; pp 231−248.
(9) Peijs, T. *Materials today* **2003**, *6*, 30.
(10) Kitayama, T.; Utsumi, S.; Hamada, H.; Nishino, T.; Kikutani, H.; Ito, H. *J. Appl. Polym. Sci.* **2003**, *88*, 2875.
(11) Turbak, A. F. *Tappi J.* **1984**, *67*, 94.
(12) Alexander, L. E. *X-ray Diffraction Methods in Polymer Science*; John Wiley & Sons: New York, 1969; Chapter 7.
(13) Nishiyama, Y.; Langan, P.; Chanzy, H. *J. Am. Chem. Soc.* **2002**, *124*, 9074.
(14) Nielsen, L. E. *Mechanical Properties of Polymers and Composites*; Marcel Dekker Inc.: New York, 1975; Chapter 8.
(15) *CRC Handbook of Chemistry and Physics*; Lide, D. R., Ed.; CRC Press: Boca Raton, FL, 2003; 12−219.

MA049300H